Technical Design Report of BASE-STEP

Christian Smorra[1,2]*, Steffen Gavranovic*[1]*, Daniel Popper*[1]*, Stefan Ulmer*[2]*, Jack Devlin*[2,3]*, Yann Dutheil*[3]*, Barbara Latacz*[2]*, Elise Wursten*[2,3]*, Matthew Bohman*[2,4]*, Matthias Borchert*[2,5]*, Stefan Erlewein*[2,3]*, Valentin Grunhofer*[1]*, Markus Wiesinger*[2,4]*, Klaus Blaum*[4]*, Yasuyuki Matsuda*[6]*, Andreas Mooser*[2,4]*, Christian Ospelkaus*[5,7]*, Wolfgang Quint*[8]*, Jochen Walz*[1,9]*, Yasunori Yamazaki*[2]

[1] Institute of Physics, Johannes Gutenberg University Mainz, Mainz, Germany
[2] Fundamental Symmetries Laboratory, RIKEN, Wako-shi, Japan
[3] CERN, Geneva, Switzerland
[4] Max Planck Institute for Nuclear Physics, Heidelberg, Germany
[5] Leibniz Univeristät Hannover, Hannover, Germany
[6] University of Tokyo, Komaba, Japan
[7] Physikalisch Technische Bundesanstalt, Braunschweig, Germany
[8] GSI Helmholtzzentrum für Schwerionenforschung, Darmstadt, Germany
[9] Helmholtz Institute Mainz, Mainz, Germany

Abstract

BASE-STEP is a transportable antiproton trap system with the purpose to improve tests of CPT invariance based on antiproton precision measurements. The magnetic field fluctuations in the AD/ELENA facility impose a major limitation in upcoming antiproton CPT invariance tests, and BASE-STEP enables to circumvent these limitations and relocate antiproton precision measurements into a calm magnetic environment. This documents describes the technical design of the BASE-STEP apparatus and its proposed implementation in the AD/ELENA facility.

Keywords

CERN report; technical design report; ELENA; BASE; STEP; antiproton; transportable trap

CERN-SPSC-2021-007 / SPSC-TDR-007
18/03/2021

1 Physics Motivation

The Standard Model of particle physics leaves us currently with unsatisfying explanations for the matter-antimatter asymmetry and the existing dark matter in our universe [1, 2], which inspires many experimental searches for new physics including precision measurements at low energies [3]. This approach of testing the Standard Model covers so far only very few precision tests on antiparticle systems, with the most significant contributions coming from the research community at the Antiproton Decelerator of CERN [4], covering antiprotonic helium spectroscopy [5], antihydrogen spectroscopy [6–8], and the high-precision measurements of the antiproton's fundamental properties [9, 10].

The BASE collaboration has performed the to-date most precise antiproton precision measurements. These measurements improved the limits on a potential proton-to-antiproton charge-to-mass ratio difference and test the weak equivalence principle for antimatter [10]. Further, BASE provided a 3000-fold improved limit on potential CPT-violating effects based on the magnetic moment difference of a single proton and a single antiproton [9, 11], and the first limits on time-dependent CPT violating effects and the antiproton coupling to axion-like dark matter [12]. Our measurements have confirmed the Standard Model up to the current level of precision reaching up to 69 ppt in relative precision and down to 5×10^{-25} GeV in energy resolution of a modified level splitting in the artificial atom formed by the single antiproton in the Penning trap [13]. Since we are still lacking an explanation for dark matter and the matter-antimatter asymmetry based on our current experimental observations, this requires further

exploration of the limits of the Standard Model and to search with increased experimental precision in our measurements.

The project BASE-STEP (Symmetry Tests in Experiments with Portable antiprotons) provides a stepping stone towards improving the sensitivity on potential CPT violating effects in the baryon sector and other beyond Standard Model couplings for the next generation of antiproton precision measurements. These will require a higher magnetic field stability than presently available in the AD/ELENA facility, where we are expecting to measure at the edge defined by the external magnetic field noise in the upcoming magnetic moment and charge-to-mass ratio measurements until LS3. BASE has demonstrated that we can measure cyclotron frequency ratios 5-times more precise when the other operations in the AD/ELENA facility are on hold [14]. Consequently, our collaboration intends – as outlined in our recent experiment proposal [15] - to relocate antiproton precision measurements from the AD/ELENA facility into a calm magnetic field environment using a dedicated precision laboratory for our future measurements.

The key method enabling these measurements will be the availability of the transportable antiproton trap BASE-STEP, and we intend to construct, commission, and demonstrate all the essential methods to operate such transportable traps latest until the start of LS3. BASE-STEP will be a compact transportable antiproton trap only featuring the essential components for the transport, and an ejection system, which allows to transfer the stored antiprotons into a precision Penning trap system outside the AD facility. Depending on official regulations regarding the transport on public roads, it may also become possible to supply other similar experiments with antiprotons, such as the other BASE experiments outside of CERN in Hannover [16] and Mainz [17], radiofrequency traps [18], or other upcoming experiment ideas. It will also become possible to utilize the transportable trap for antihydrogen ions $\overline{H}^+$ [19,20], the antihydrogen molecular ion $\overline{H}_2^-$ [21,22], or highly-charged ions from HIE-ISOLDE which are difficult to produce in non-accelerator environments [23].

Regarding additional physics objectives, the BASE-STEP trap system can perform dedicated lifetime measurements in the transportable trap as outlined in reference [24], and enable the possibility to make simultaneous antiproton cyclotron frequency measurements with uncorrelated noise in the course of expanding the search for antiproton dark matter coupling, which could reveal topological defects in dark matter, e.g. through a quadratic dark matter-antiproton coupling to the antiproton mass [25]. In addition, red-shift experiments using the antiproton cyclotron frequency and an active modification of the gravitation potential may become possible in the future [26].

2 Magnetic field limitations and requirements for antiproton precision measurements

Our limits on beyond Standard Model physics effects stem from frequency measurements of single trapped particles in our cryogenic advanced multi-Penning trap system [27], in particular of the antiproton's Larmor (spin-precession) frequency and the cyclotron frequencies of antiprotons and the negative hydrogen ion:

$$\nu_{L,\bar{p}} = \frac{1}{2\pi}\frac{g_{\bar{p}}}{2}\left(\frac{q}{m}\right)_{\bar{p}} B \tag{1}$$

$$\nu_{c,\bar{p}} = \frac{1}{2\pi}\left(\frac{q}{m}\right)_{\bar{p}} B \tag{2}$$

$$\nu_{c,H^-} = \frac{1}{2\pi}\frac{1}{R}\left(\frac{q}{m}\right)_{p} B. \tag{3}$$

Here, $R = 1.001\,089\,218\,754(2)$ is the mass ratio of the negative hydrogen ion to the proton [10] in a magnetic field of $B = 1.944864\,\mathrm{T}$, q and m denote the charge and mass of the particles, and B is the magnetic field in the trap. In particular, we compare the proton and antiproton charge-to-mass ratios, and

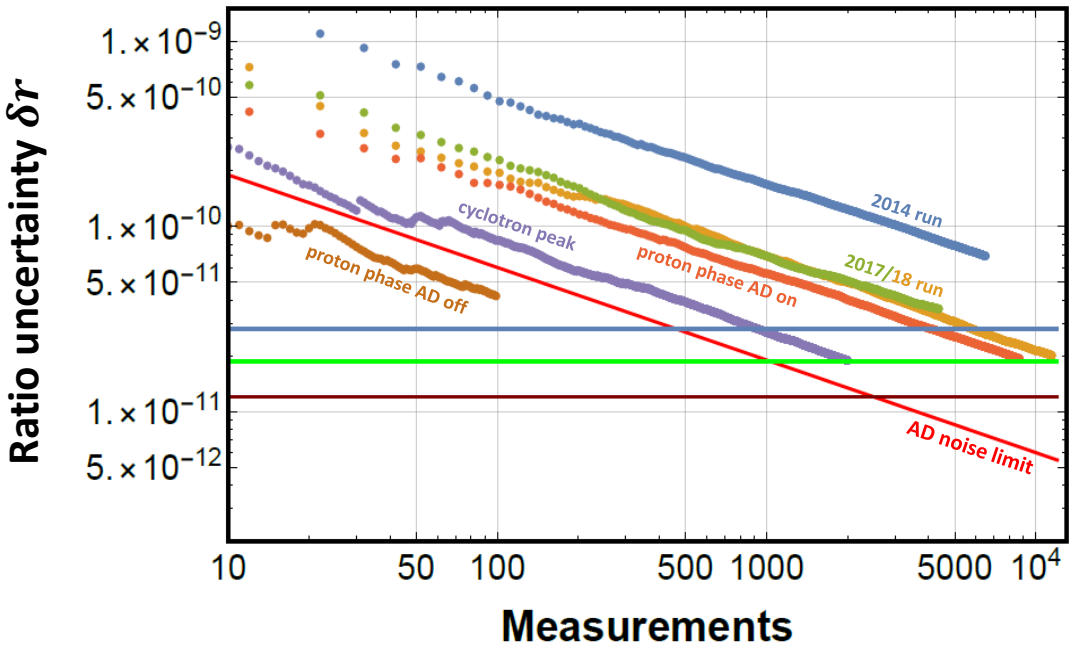

Figure 1: Uncertainty of measured cyclotron frequency ratios as function of the number of measurements under different measurement conditions [14]. The limit imposed by the periodic magnetic field ramps of the antiproton decelerator is inferred from magnetic field sensor data in the BASE experiment area and shown as red line. Most importantly, the red dots and the brown dots represent the difference in precision with the same measurement method with and without the magnetic field noise in the AD/ELENA facility showing the permanent improvement that can be gained from relocating the antiproton precision measurements into a calm magnetic environment.

determine the antiproton magnetic moment by measuring the frequency ratios:

$$\frac{(q/m)_{\overline{p}}}{(q/m)_p} = \frac{1}{R}\frac{\nu_{c,\overline{p}}}{\nu_{c,H^-}} \tag{4}$$

$$\mu_{\overline{p}}/\mu_N = \frac{g_{\overline{p}}}{2} = \nu_{L,\overline{p}}/\nu_{c,\overline{p}}, \tag{5}$$

respectively. Here, $g_{\overline{p}}$ is the antiproton g-factor, which expresses the magnetic moment of the antiproton in units of the nuclear magneton μ_N.

Notably, the magnetic field cancels exactly in an ideal measurement, which means in turn that we can apply our method up to the limit that is imposed by magnetic field fluctuations during the measurement. Our trap system is configured to provide the highest possible magnetic field stability by using a superconducting magnet in persistent mode [28], using advanced superconducting self-shielding solenoids for shielding [29, 30], and various efforts to decouple other environmental effects (helium tank pressure, temperature fluctuations, etc.) from changing the magnetic field in the trap. These experimental efforts have been intensified after completing the first parts-per-billion antiproton magnetic moment measurement, in order to improve the charge-to-mass ratio comparison as much as possible [14]. In the course of this work, we characterize the impact of magnetic field fluctuations by using the cyclotron-frequency ratio scatter of subsequent cyclotron frequency measurements:

$$\sigma_r = \sigma\left[\nu_{c,2i}/\nu_{c,2i-1}\right]_{i=1}^{N}, \tag{6}$$

where σ denotes the standard deviation, and $\nu_{c,i}$ is a series of cyclotron frequency measurements resulting in N frequency ratios of either the same trapped particle, or of alternating measurements of two

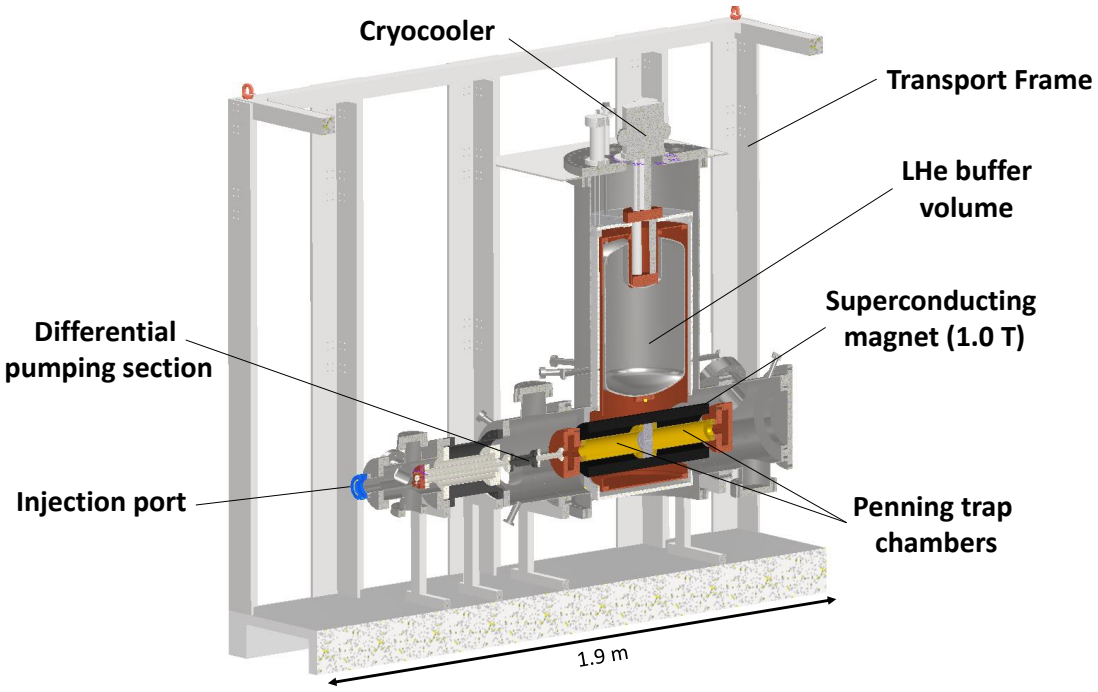

Figure 2: Cut view of the BASE-STEP apparatus for transporting antiprotons.

different particles. Assuming normal-distributed data, we expect to reach $\delta r = \sigma_r/\sqrt{N}$ as uncertainty on the frequency ratio after N ratio measurements. Such measurements have been performed in our recent charge-to-mass ratio comparisons, and while testing the performance of new cyclotron measurement methods with protons. We reproduce here for convenience the latest summary of the collected cyclotron frequency ratio in our annual report from 2019 in Fig. 1 [14]. We can infer the stability limit of the external magnetic field noise on the cyclotron frequency stability based on the magnetic field fluctuations in the experiment zone and the shielding factor of our advanced self-shielding solenoid system [29]. This limit is shown in Fig. 1 as red line. Our measurements during the operation of the AD/ELENA facility have reached a stability close to this limit. Furthermore, we can compare the performance of the recently developed proton cyclotron phase measurements with and without operation of the antiproton decelerator, which shows a factor of 5 improvement without the periodic magnetic field ramps of the antiproton decelerator. Under this condition, the BASE trap system reaches at the moment $\sigma_r \sim 280\,\text{ppt}$, which can likely be further improved by stabilizing the (magnetic) environment, since other experiments in precision laboratories have already demonstrated $\sigma_r < 100\,\text{ppt}$ in their dedicated cyclotron-frequency ratio measurements [31–34]. At this performance, we require one month of measurement time without magnetic activities in the AD/ELENA facility to reach a relative precision of 5 p.p.t. In addition, we also require the same stable measurement conditions to prepare and characterize the apparatus and to conduct systematic studies. Finally, we note that further shielding of the high in-trap magnetic field is challenging even with advanced compensation systems [29], and if we would succeed in further shielding improvements that combining lower external magnetic field fluctuations and the optimized shield potentially even improves the measurement precision in precision laboratories further. Therefore, it is of great advantage to conduct future antiproton precision measurements outside the AD hall where continuous development and operation of the experiment can take place without interference with other operations.

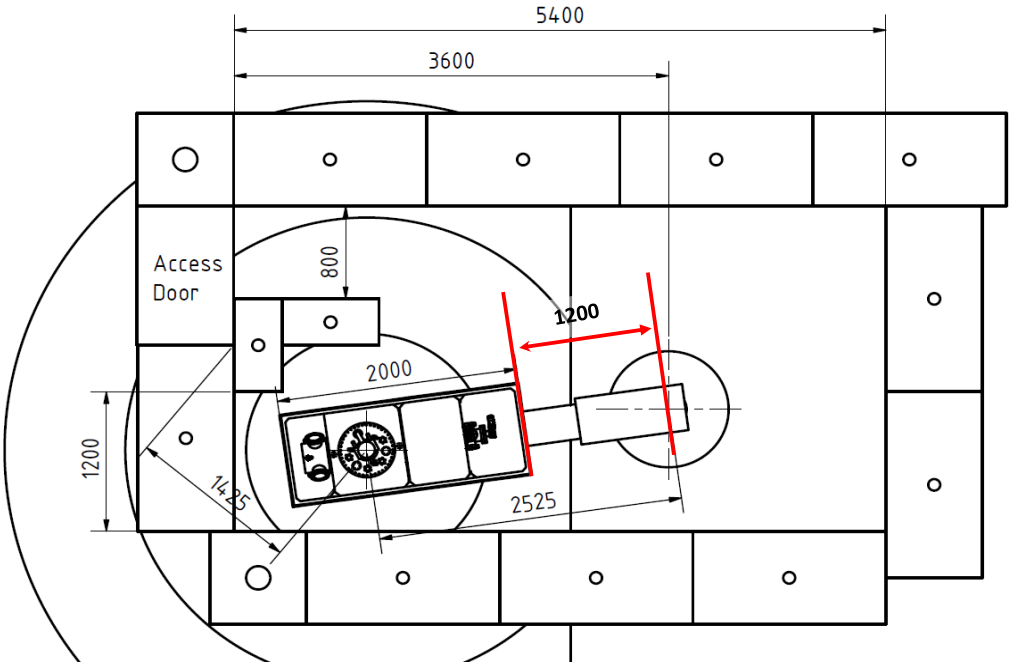

Figure 3: Layout of the modified ATRAP I zone for the operation of the BASE-STEP apparatus. The modified concrete radiation shielding, the BASE-STEP apparatus, the beamtube and the 90 degree deflector connecting to the vertical handover point are shown.

3 The experimental apparatus

3.1 Overview

The BASE-STEP apparatus is shown in Fig. 2. It consists of a transportable superconducting magnet with 1 T magnetic field with a horizontal bore containing a two-Penning trap system. The superconducting magnet is a cold-bore magnet with a common cooling system for the superconducting coils and the Penning trap system in the bore. Its primary cooling power comes from a cryocooler for stationary operation or while connected to a mobile power generator, and a liquid helium buffer tank as secondary cooling mechanism to bridge time where no power is available during the transport. Consequently, BASE-STEP can operate during the craning and for transporting on short distances without large power UPS and battery systems. The magnet bore contains a separate cryogenic vacuum chamber with two cryogenic traps that are connected via a differential pumping section to the injection port. The latter will be attached to the ELENA beamline for loading antiprotons, and forms also the exit for transferring antiprotons into a precision measurement trap system. Details on the design of the differential pumping section are reported below since the vacuum conditions in the traps are crucial for the success of the project - antiprotons have a trap lifetime of about 5 s at a residual gas pressure of about 10^{-10} mbar, and we require a vacuum of at least 10^{-16} mbar for about three month trap lifetime to be able to conduct precision measurements offline.

For the sake of portability, we designed the transportable trap system as compact as possible. The transportable magnet cryostat and the differential pumping section are installed on an aluminum transport frame with dimensions 2.00 m length, 0.90 m width, and 1.85 m in height. The system can be transported by fork lift and overhead crane, in particular also through the top floor exit in the AD hall to the parking lot outside the AD. We aim for a total weight below 1000 kg in total for the aluminum frame, which will contain the entire equipment needed for the transportable trap, except for the cooling-water chiller system, which is foreseen to be placed on a separate transportable rack and is required to cool the compressor of the cryocooler during transportation.

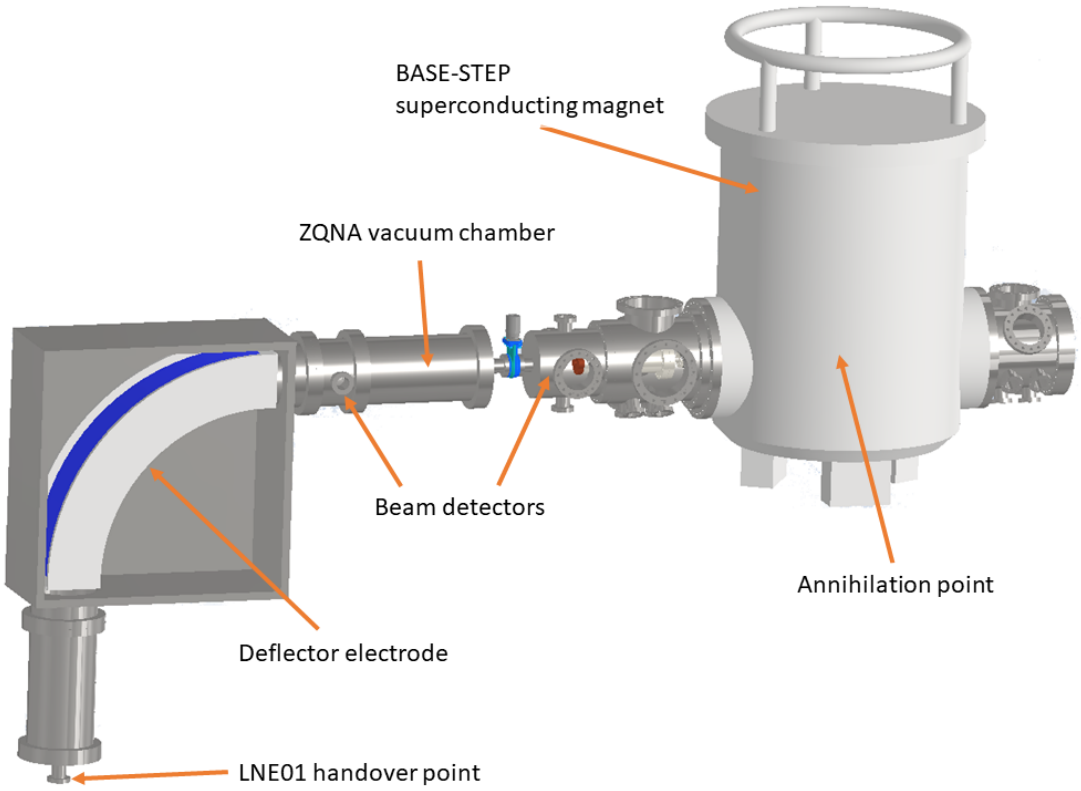

Figure 4: Vacuum chambers of the BASE-STEP beamline and the transportable trap.

We intend to place BASE-STEP at the former ATRAP I ejection port, as shown in Fig. 3. The ATRAP I zone has a vertical ejection port, however, BASE-STEP is a horizontal Penning trap, since a vertical setup would be impractical for the transport considering the overall length needed along the axis for the trap system and the differential pumping section. Therefore, the experiment zone requires some modifications of the radiation shielding, and an extension of the antiproton ejection beamline. We will use a 90 degree electrostatic deflector and additional quadrupole doublets to bridge the gap to the handover point and inject the antiprotons from ELENA into BASE-STEP.

The following sections describe the technical details of the BASE-STEP apparatus, and its installation and operation in the former ATRAP I zone.

3.2 Design of the ejection beamline for BASE-STEP at the former ATRAP I ejection

The injection of antiprotons into BASE-STEP requires to extend the ELENA ejection beamline up from the present handover point in the ATRAP I zone by a 90 degree deflector, followed by additional focusing and steering elements. These additional parts will be designed and prepared by the BASE collaboration. The system of vacuum chambers, which needs to be connected to the handover point is shown in Fig. 4.

ELENA has not made use of 90 degree electrostatic deflectors so far, therefore the design of existing ZDSV deflectors needs to be adapted for this purpose. We have constructed a model for the electrodes of the 90 degree electrostatic deflector using two concentric spherical plates with a nominal bending radius of 600 mm, 60 mm spacing between the electrodes and a height of 180 mm. The nominal bending voltages are ± 10 kV for the deflector electrodes, identical to the nominal voltages of the existing ZDSV designs. The high-voltage electrodes are surrounded by grounded plates on the top and bottom, and by entrance/exit plates which have apertures with the same shape as the free space between the spherical electrodes. The electrode geometry including the grounded shielding plates is shown in Fig. 5. We have used COMSOL to compute the electric field between the two deflector plates, and to determine

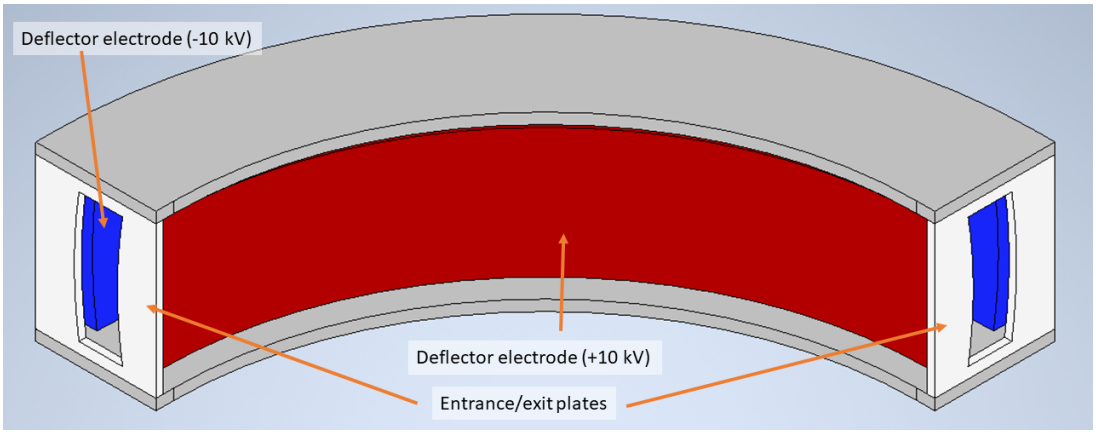

Figure 5: 3D model of the deflector electrodes in red and blue, and the surrounding grounded plates (light and dark grey).

the transfer matrix of the deflector by particle trajectory calculations. The resulting transfer matrix is:

$$\begin{pmatrix} X_o \\ X'_o \\ Y_o \\ Y'_o \\ T_o \\ Z'_o \end{pmatrix} = \begin{pmatrix} -0.2413(37) & 0.5445(28) & 0.0064(9) & 0.0005(16) & 0 & -0.0002(15) \\ -1.592(4) & -0.285(4) & -0.0077(5) & -0.0140(22) & 0 & -0.014(4) \\ 0.008(7) & -0.002(4) & -0.357(4) & 0.554(8) & 0 & 1.592(4) \\ -0.008(4) & -0.004(6) & -1.6906(28) & -0.294(8) & 0 & 1.991(7) \\ -134.54(26) & -108.8(5) & -0.5(7) & 0.29(19) & 1 & 373(19) \\ -0.0002(20) & 0.0001(6) & 0.0002(24) & 0.0003(7) & 0 & 1.0004(25) \end{pmatrix} \begin{pmatrix} X_i \\ X'_i \\ Y_i \\ Y'_i \\ T_i \\ Z'_i \end{pmatrix} . \quad (7)$$

The coordinates X, Y and angles X', Y' are given in the local reference frame moving along the beam trajectory, and $T = -c\Delta t$ describes the offset along the reference trajectory, and Z' is the ratio of the particle velocity along the reference trajectory to the one of the reference particle. The matrix includes two drift sections of 0.19 m and 0.20 m at the entrance and exit of the deflector, respectively. We found that the fringe field at the entrance and exit of the deflector causes deviations in transfer matrix compared to an ideal deflector and in addition non-linear effects. The present geometry has reduced the non-linear contributions to the level of the uncertainties in the entries of the transfer matrix, being at the relative level of about 10^{-3} for the non-zero elements. The non-linearities are smaller compared to circular apertures, and additional fine tuning is possible e.g. by changing the curvature radius of the electrodes, and changing the thickness and position of the entrance and exit plates.

This matrix was included into a MAD-X model that extends the LNE 01 extraction line up to the trap center of BASE-STEP without changes to the existing LNE01 extraction to simulate the beam transfer into BASE-STEP. The results of these computations are shown in Fig. 6 (Yann Dutheil kindly carried out these studies). The maximum RMS beam diameter along the trajectory is less than 5 mm and the maximum quadrupole voltage for these settings are below 4.3 kV, which is well within the specifications of the ZQNA elements. BASE-STEP will use two sets of Faraday plates with charge amplifiers to steer the beam into the trap center. These systems have been previously used by the BASE collaboration for steering in the main experiment. The focal point at the trap center has an RMS size of 0.53 mm in the horizontal, and 1.00 mm in the vertical plane. This is smaller than the acceptance range for catching of the BASE-STEP trap system, which is about radially 2 mm around the trap center.

We conclude that the presented calculations show that BASE-STEP can be supplied with antiprotons in the former ATRAP I zone using the presented beamline layout, and that the space in the proposed zone layout is sufficient to install these elements. BASE will manage the production of the 90 degree deflector. We would appreciate the possibility to use a spare ZQNA element from the ELENA team, if this is not possible, we will reproduce a similar element based on the electrode geometry of the ZQNA element. The beamline elements are planned to be available in March 2022.

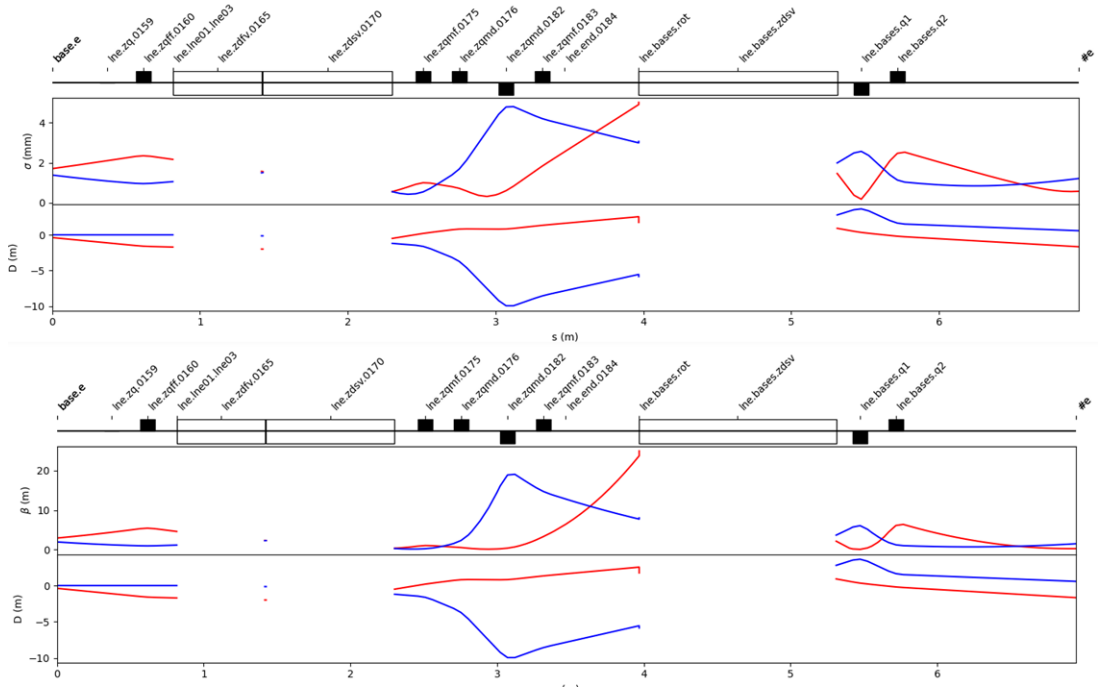

Figure 6: Results of the MAD-X simulation of the BASE-STEP ejection line. The RMS beam diameter and optical functions for the X and Y coordinates are shown. The functions are omitted inside the vertical kicker and deflector, since MAD-X does not compute the evolution of the beam inside these elements.

3.3 Transportable superconducting magnet

The transportable superconducting magnet will be a key component in the experimental apparatus of BASE-STEP. Compared to common stationary NMR-type magnets, the BASE-STEP magnet will use a hybrid cooling concept using a cryocooler backed up by a liquid helium tank. The cryocooler is the primary source for cooling power. We use a two-stage cryocooler with 45 W cooling power at 50 K on the first stage, and 900 mW cooling power on the 4 K stage to cool the heatshields, the superconducting magnet coil and the Penning trap system. It has a power consumption of 8 kVA which is supplied from the power grid in stationary operation and by a power generator in case of long transport times. The liquid helium tank has a volume of 30 L and can keep the system cold when transporting short distances without power. The present estimated heat load on the second stage of the cryocooler is about 350 mW in thermal equilibrium, and about 1.2 W heat conductance through the cold head are added when the cryocooler is switched off. From these values we anticipate a liquid helium standing time of eight hours after the cryocooler loses power, which will suffice to move the magnet system by crane out of the AD/ELENA facility, and even to relocate to a different laboratory at CERN without a mobile power source for the cryocooler. Other essential equipment, such as the trap voltage (15 W), temperature, pressure and liquid helium sensors (50 W) can be supplied with low power UPS batteries. An additional advantage of the cryogenic setup is that the magnet and the experiment share the same cooling system. This avoids the need for a second cryocooler or cryostat and results in a very compact installation. Further, the magnet features a recondensing system for the liquid helium tank, so that its consumption in stationary operation is zero. The recondenser can also be used to fill the liquid helium tank by inserting high-purity helium from a gas bottle into the LHe tank. Occasional fills with about 30 L of liquid helium would be necessary for transporting or after starting up the system and can be obtained from the liquid helium supplies of the BASE main experiment.

An additional requirement for the superconducting magnet system is that it needs to withstand the mechanical stress during the transport while cold and in operation. Conventional NMR-magnets are

shipped warm and uncharged, and usually have an additional demountable mechanical support for the transport to prevent damage on the cold stage from acceleration and shocks. The mechanical construction of the transportable trap cryostat uses a network of G10 rods to support the cold stages, which is designed to withstands forces up to 1 G in all directions. Thereby, the device fulfills the CTU standards (packing of Cargo Transport Units) for shipping by truck. Further, stray fields of the magnetic field are suppressed by a carbon steel vacuum chamber surrounding the setup, so that magnetic field drops to below 0.5 mT outside the transport frame. Consequently, there are no magnetic hazards due to stray fields during the transport.

The superconducting coil of the magnet provides a 1.0 T magnetic field in a cold bore of 100 mm diameter. The magnet will operate in persistent mode, so that a current source is not required during the transport. The homogeneous center of the magnet is 150 mm long and 5 mm in diameter, and features low magnetic field gradients with the linear and quadratic gradients being below 10 mT/m and 5 T/m^2, respectively, so that image-current detection can be performed in two separate traps without significant line-width contributions from the residual magnetic field inhomogeneity. The choice of the magnetic field strength is related to the electron cooling time constant, since efficient electron cooling is the initial step for preparing cold antiprotons in our trap. The cyclotron cooling time constant is about 1 s in a magnetic field of 1 T, and these parameters suffice in other experiments to prepare and trap large amounts of cold antiprotons.

The magnet production is being performed by *Bilfinger Noell*. The contract for production started in September 2020 and the design studies were completed in November 2020. The design documents are confidential and therefore not included in this report. The latest delivery date for the magnet system is April 2022, but the project planning at Bilfinger presently shows that delivery in late 2021 is possible. BASE-STEP will be commissioned following the delivery of the magnet in the experiment zone.

3.4 Trap system

The trap system of the transportable trap is located in the cold bore of superconducting magnet with 1.0 T magnetic field strength. It consists of two electrode stacks separated in two cryogenic chambers as shown in Fig. 7. Both traps are connected by a transport channel for transferring the antiprotons between the two trap systems. The first trap is named the vacuum lock trap (VLT), since its most essential function is to be a vacuum lock to protect the vacuum conditions in the reservoir trap (RT) while the vacuum lock trap is opened to the injection port for catching or transferring antiprotons (see below for further details). All electrodes shown here are gold-plated OHFC copper electrodes with an inner diameter of 12 mm. Compared to the BASE trap system with 9 mm diameter [27], the increased trap dimensions allow potentially to accumulate more antiprotons. The electrodes are spaced by sapphire rings which provide electrical insulation but good thermal conductance.

In the following, we describe the functionality of the trap system. The VLT is equipped with the established equipment for loading antiprotons from the AD/ELENA ejection lines. A set of catching electrodes at both ends of the electrode stack is used to apply catching HV pulses to provide the initial confinement. A cryogenic field emission point provides electrons that are stored in one of the harmonic potential wells in the VLT and sympathetically cool antiprotons close to the cryogenic environment temperature. The next step in our loading procedure is the electron cleaning, and the initial preparation of an antiproton cloud in the trap system based on methods established earlier [27].

The most important function regarding economic use of the stored antiproton is the implementation of the separation and merge procedures that where first applied in the BASE reservoir trap [38]. These allow to non-destructively separate a cloud of antiprotons into two fractions and count their respective size by using the image current detector. For this purpose, the VLT will be equipped with an axial resonator (500 kHz) and a cyclotron resonator (15 MHz) to detect the image currents of the trapped antiprotons and determine the number of trapped antiprotons in both fractions of the cloud. The detection system is connected next to the center ring electrode of the trap for efficient detection in the main trap

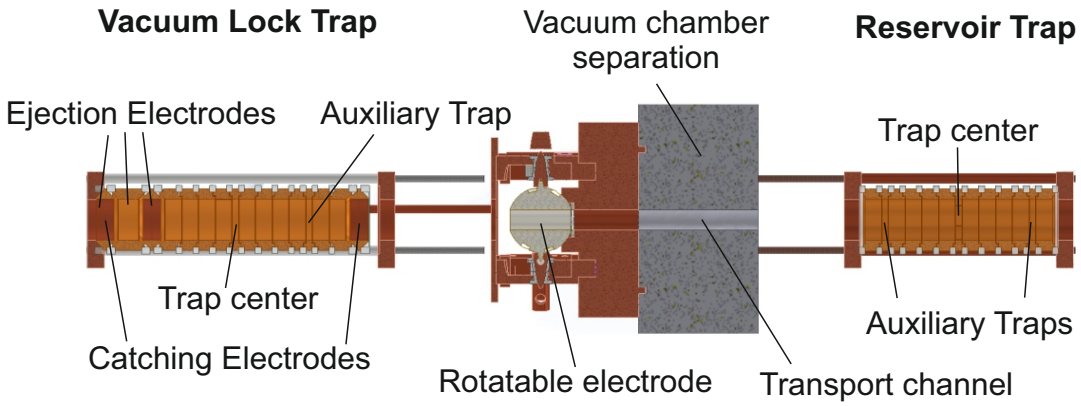

Figure 7: Cut view of the STEP trap system.

region, which has an optimized harmonic potential for detection of single particles. The trap stack also contains a second auxiliary trap that provides a similar electric field configuration to the main trap for detection, but has less possibilities for particle manipulation. In comparison to the BASE reservoir trap, the auxiliary detection region permits the simultaneous detection of the two separated fractions in the main and auxiliary traps, which accelerates the preparation time by a factor of 2.

The VLT is also equipped with electrodes which permit fast pulses to transfer of antiprotons either to the RT or into a second trap system that is attached to the injection port after relocating the trap system from ELENA to the offline laboratory. BASE usually transports antiprotons adiabatically along the magnetic field lines using slow voltage ramps with $\tau \approx 100\,\mathrm{ms}$ filter time constant. Here, we use instead the "ballistic" transport, where the trap potentials at both ends of the transfer distance are opened and closed by voltage pulses and the antiprotons are accelerated and decelerated by an electrostatic potential. These methods are routinely used in other Penning trap experiments, for example at SHIPTRAP, which has two traps separated by a differential pumping barrier in the same superconducting magnet, and ions are transferred here between the traps with low acceleration voltages $< 100\,\mathrm{V}$ [39]. This concept will be applied in the BASE-STEP trap system for the VLT to RT transfer. Regarding the transfer into a second trap system, higher acceleration voltages are required. Therefore, the VLT is equipped with three ejection HV electrodes at the side of the trap that is connected to the room temperature vacuum chamber. These electrodes allow to float the trap potential up to -3 kV to provide the acceleration voltage for the antiprotons. A similar transport concept is used in ISOLTRAP at ISOLDE, which performs electrostatic transport between the two traps in two separate superconducting magnets with about 3 kV acceleration voltage [40]. In comparison, BASE-STEP requires to transfer the antiprotons through the two differential pumping sections of its own and the target trap system and requires a smaller transverse displacement of the particle trajectories. The ion optics transfer system for this purpose is presently still in the design phase.

The second trap, the RT, implements essentially features of the non-portable BASE reservoir trap, which was very successfully used from 2014 until LS2 and enabled antiproton precision measurements with very low beam demand and up to 405 days autonomous experiment operation [24]. BASE-STEP has improved on the original concept by using a main trap and two auxiliary traps, so that antiprotons can be detected in three separate potential wells. In addition, the trap is equipped with a rotating wall, to potentially enable storing antiprotons even at particle numbers in the plasma regime. The separate cryogenic vacuum chamber provides additional protection from incoming residual gas through the transfer section.

The trap electrodes for the entire trap system have been machined, and the assembly of the VLT electrodes before gold plating is shown in Fig. 8. The remaining parts of the cryogenic trap system (pinbase and trap chambers) are currently in preparation. The first axial detection system for the trap

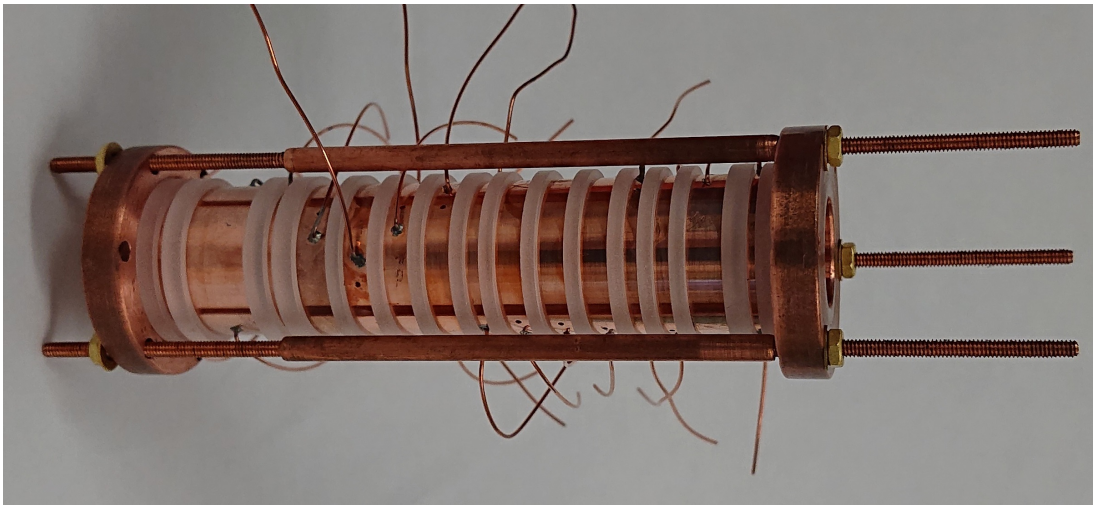

Figure 8: Photograph of the electrodes of the vacuum lock trap before gold plating.

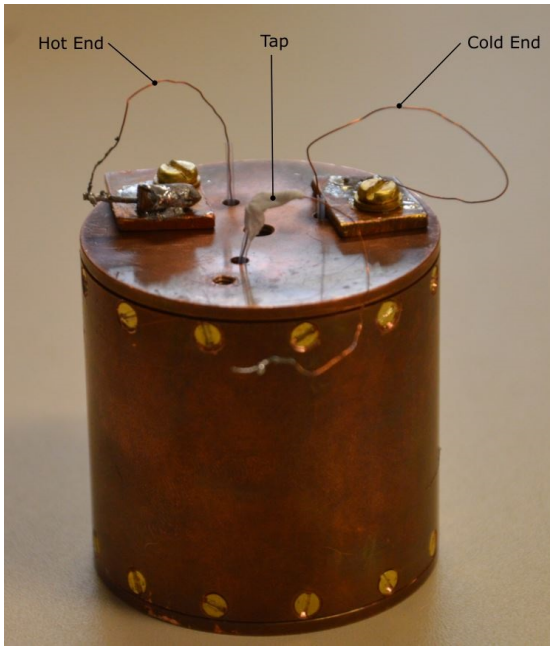

Figure 9: Picture of the axial resonator for the vacuum lock trap of BASE-STEP.

system has also been commissioned and characterized. The design is based on our previous experience on antiproton image-current detectors [41]. Here, we use here a NbTi coil in a copper housing as resonator, and an amplifier based on the dual-gate GaAs FET 3SK177 with the layout described in reference [42]. The requirements on the detection system are not as stringent as for the precision measurements or the spin-state detection in the BASE apparatus, therefore we forfeit the superconducting housing lowering the Q-value of the unloaded circuit to $Q \approx 40\,000$, sufficient for single particle detection but gaining a more reliable thermalization. A photograph of the resonator is shown in Fig. 9. With the amplifier and trap connected to the detection system, we obtain a Q-value of $Q = 19\,000$, a S/N of 28 dB, and a single particle dip-width $\Delta\nu = 3.6\,\text{Hz}$, which is more than sufficient for the requirements described above. A second axial detection system is currently in production. Further, it is planned to equip the trap system with two cyclotron detectors at $\nu_+ \approx 15\,\text{MHz}$ to have the possibility to observe the trapped particles also via the cyclotron mode, which would also provide additional diagnostics, e. g. for lifetime studies.

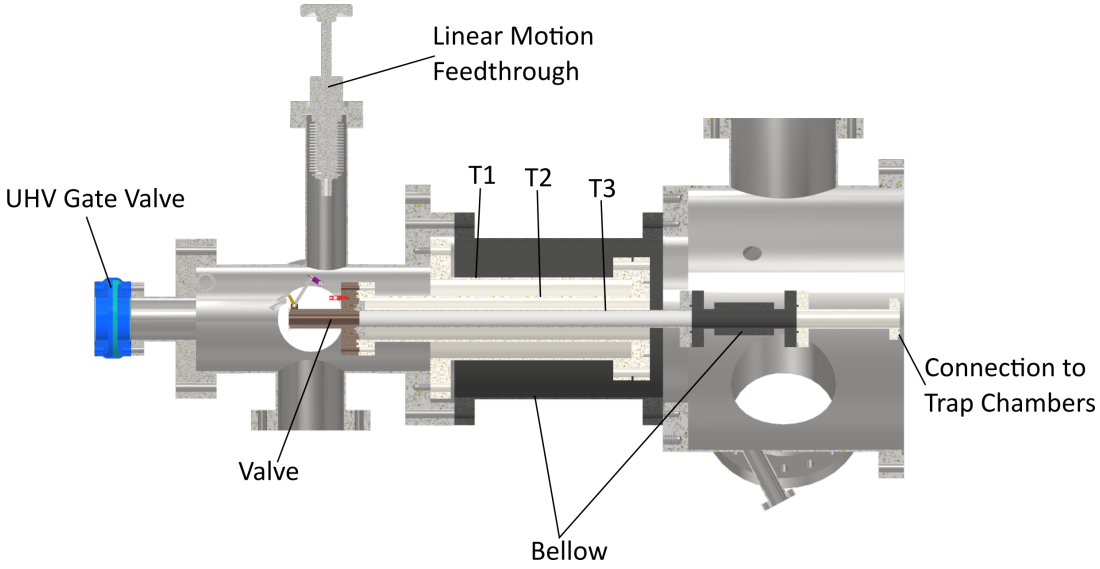

Figure 10: Cut view of the differential pumping section. The antiproton injection is connected to the UHV gate valve on the left, and the vacuum lock trap chamber is connected at the right. The tubes T1, T2 and T3 separate the magnet cryostat isolation vacuum and the inlet chamber vacuum on the left and contribute to the heat and gas flow resistance into the trap chambers.

3.5 Differential Pumping Section

The most crucial aspect in the design of the transportable trap is to ensure excellent vacuum conditions in the cryogenic trap chambers, since a pressure $p = 10^{-16}$ mbar is required to obtain a trap lifetime of 3 months. So far, BASE has injected antiprotons through thin vacuum windows into a hermetically-sealed cryogenic vacuum chamber [27], where we could place an upper limit on the vacuum of better than 10^{-18} mbar from storing antiproton clouds up to 405 days in the BASE trap system [24].

An open cryogenic trap system requires several mechanisms to protect the antiprotons from annihilation with residual gas. First of all, it requires excellent room temperature vacuum conditions at the inlet to the trap chamber. To this end, we separate the inlet vacuum chamber and the magnet cryostat isolation vacuum, which is due the presence of superisolation foil and experiment electronics usually only moderately pumped ($p \sim 10^{-8}$ mbar). For this purpose, the differential pumping section is constructed also as vacuum separation between the cryostat isolation vacuum and the inlet chamber. Since this functionality leads necessarily to a thermal path between the room temperature vacuum chambers and the cryogenic trap system, it is also designed to have a large thermal resistance by using a set of concentric titanium grade 5 tubes as thermal conduction barrier, see Fig. 11. The pieces in the top show the parts labeled as T1 and T2 in Fig. 10, and the pieces in the bottom show T3, the stainless steel bellow to counteract the thermal contraction, and the titanium part connected to the trap chamber. The later form also the conduction barrier for the molecular flow of residual gas into the trap chambers and have presently a length of about 500 mm and a free inner diameter of 16 mm. The flow conduction can be further reduced by placing an narrower channel at the entrance of the trap chamber, where the magnetic field will constrain the transverse motion of the particles during injecton and ejection. In the following, we consider only the existing part of the differential pumping section to estimate the flow resistance and the monolayer formation times in the trap system.

To reduce the particle flow into the cryogenic trap chambers, the inlet chamber will be vacuum fired to reduce the outgassing, and will be pumped using two turbo molecular pumps in series and NEG cartridges to reach at least 10^{-10} mbar in operation. The residual gas pressure in the inlet chamber causes a molecular flow of hydrogen and helium into the differential pumping barrier, which leads first

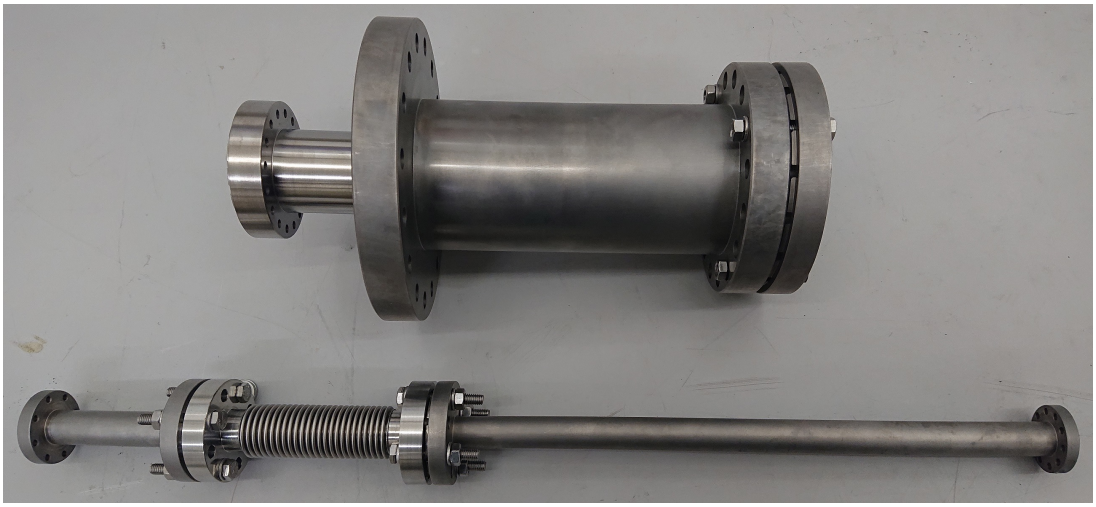

Figure 11: Photograph of the titanium tubes forming the differential pumping section.

to a monolayer formation of residual gas particles on the cold surfaces in the trap chambers, and subsequently to a pressure increase in the vacuum lock chamber. While the vacuum lock chamber can still be conveniently operated with moderate antiproton storage times of a few hours, the reservoir trap needs to remain below $p = 10^{-16}$ mbar at all times to ensure the successful operation. Consequently, the vacuum lock function of the first cryogenic trap chamber is crucial for the success of the transportable trap. This function is implemented by the inlet valve and the rotatable electrode in front of the transport channel, see Fig. 7. The inlet valve is opened for the injection and ejection of antiprotons from the VLT, and closed otherwise. The rotatable electrode opens the channel to the RT after the inlet valve is closed and after the residual gas has attached to the cold surfaces in the VLT chamber. As a result, only the time when the inlet valve is open contributes to the monolayer formation time, and this can be as short as ~ 30 min per antiproton loading attempt. Further, the RT monolayer formation starts only after the VLT trap as filled with residual gas, and only while the rotatable electrode is opened.

In the following, we estimate the time of the individual parts of the cryogenic system that is required until a monolayer of helium or hydrogen has formed on the surfaces so that pressure starts to raise. The starting condition of this study is that the inlet chamber is at 10^{-10} mbar, and the residual gas in the trap chambers has completely frozen out during the cooldown and that the monolayer fraction is initially negligible. This condition is reached by pumping the cryogenic trap chambers to below 10^{-6} mbar and closing the inlet valve before cooling down. All time limits quoted here scale proportional to the pressure in the inlet vacuum chamber, and may be further improved by increasing the pumping speed or by adding cold surfaces (a cryopump) to the inlet chamber to reach below the 10^{-10} mbar pressure level.

Once the inlet valve is opened, the residual gas will enter the tubes of the differential pumping section and start covering the surfaces. In a vacuum chamber with pressure P, the monolayer formation time can be calculated using the relation [43]:

$$\Delta T_M = \frac{1}{A_{mol} P (2\pi m k_B T)^{-1/2}}, \tag{8}$$

where $A_{mol} \sim (\pi/4)(300\,\text{pm})^2$ is the area covered by a residual gas particle based on its kinetic diameter [44, 45], k_B the Boltzmann constant, and m and T the mass and the temperature of the residual gas particles, respectively. For helium at 300 K and $P = 10^{-10}$ mbar we obtain $\Delta T_M = 5$ h. Here, we neglect the conductance along the differential pumping section, but this consideration shows that the inlet valve is essential to reduce the residual gas flow into the trap chambers since the surfaces in the differential pumping section will quickly form a monolayer coverage.

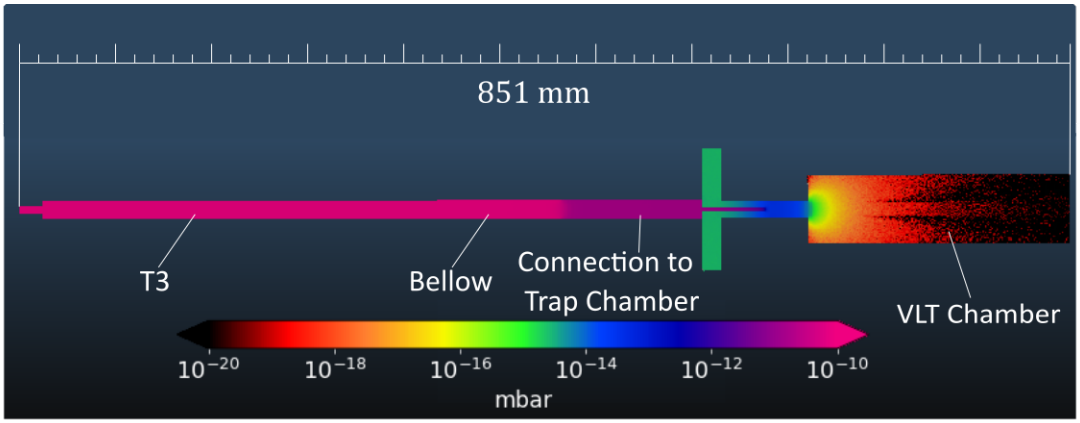

Figure 12: Pressure calculations showing the expansion of the residual gas flow into the vacuum lock trap chamber for an inlet pressure of 10^{-10} mbar. The local pressure of the incoming residual gas at the position of the vacuum lock trap in the center of the VLT chamber is below 10^{-18} mbar.

The inlet valve will be a mechanically operated cryogenic valve in the inlet vacuum chamber. The aperture of the valve is closed with a spring-loaded cover pressing on a PTFE sealing. The valve is opened with a linear mechanical feedthrough that can apply a force of up to 50 N using two pulleys. The pressure on the PTFE sealing is crucial, since this will determine the leak rate of the valve. This is important since inlet valve should provide a good protection for the trap chambers when the inlet vacuum gets worse, e.g. during the transport. An initial design for this device has been completed and a cold head cryostat with a test chamber for cryogenic valves has been prepared so that leak rate measurements can be conducted under cryogenic conditions.

If the differential pumping section is covered with a monolayer of residual gas, the residual gas will be finally entering the cryogenic trap chambers. In fact, the differential pumping section forms in this case a nozzle for an ultra-low density atomic beam source for helium and hydrogen molecules. During the injection from ELENA, we protect the antiprotons in the VLT by the degrader which is connected to a linear cryogenic piezo motor that moves the foil in and out of the trap axis. However, during the ejection, and while optimizing the beam transport to the external precision trap, the degrader foil needs to be removed. We have conducted *Molflow+* simulations to estimate the local pressure density at the position of the trap center of the vacuum lock trap, as shown in Fig. 12. Here, we observe that the pressure of the incoming gas at the trap position is negligible ($< 10^{-17}$ mbar) and that losses will only occur once the monolayer coverage in the trap chamber has increased.

For the calculation of the monolayer formation time in the vacuum lock trap, we consider the conductance of the differential pumping section to estimate the flow of particles into the VLT chamber. The differential pumping section is a thin channel connected to an ideal pump formed by the cold walls of the VLT chamber, and to a pressure reservoir of 10^{-10} mbar at the other end. Based on the particle flow through the channel, we obtain the monolayer formation time as:

$$\Delta T_M = \frac{A_{trap}}{A_{mol}} \frac{k_B T}{\Delta P\, C}, \tag{9}$$

where A_{trap} is the surface area of the trap, and ΔP and $C = 38(D^3/L) \times (T/M)^{1/2}\,\mathrm{m}^3\ \mathrm{s}^{-1}$ are the pressure difference along the channel and the conductance of the channel, respectively, with diameter D and length L in meters. We estimate ΔT_M to be at least 14 days depending on the exact temperature distribution of the gas in the channel. This is the time window in which the inlet valve can be kept open before the pressure starts to raise in the VLT trap. Since this is not equivalent to the total operation time, this is in principle sufficient to relocate antiprotons into a different trap system once all the routines are

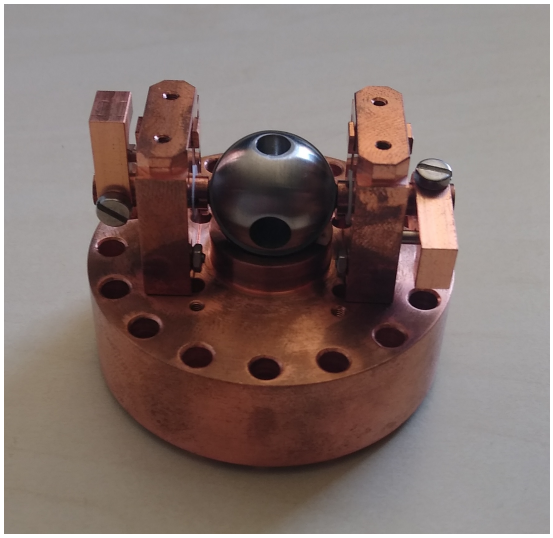

Figure 13: Picture of the rotatable electrode before wiring.

established. Here, we would need a few 30 minute attempts for loading antiprotons, and a few days of operation for the transfer into the second trap system, where we would need to first establish the transport of other ions between the VLT and the second trap system, which requires the inlet valve to remain open. The time window of 14 days can be increased by increasing the absorbing surface in the VLT chamber e.g. using charcoal surface adsorption or other porous materials to extend the operation time, and by reducing the channel diameter of the differential pumping section once the beam transport for low-energy ejection of antiprotons has been optimized.

With these considerations, it is however also clear that it is necessary to have an additional layer of protection for the vacuum conditions of the reservoir trap. Therefore, the reservoir trap has a separated vacuum chamber with a connection that is opened and closed by a rotatable electrode. The design of this electrode is based on a concept earlier used by the ATRAP collaboration [46], and uses a conductor loop to rotate the electrode in the magnetic field of the trap. We have constructed and successfully conducted the first tests of the rotatable electrode shown in Fig. 13 at room temperature in a magnetic field of 1.9 T. Our present developments focus on improving the bearing and the sealing mechanism of the electrode for cryogenic tests.

If the rotatable valve is opened and the VLT chamber pressure has already increased, we observe the same scenario for the residual gas entering into the RT chamber as for the atomic beam going into the VLT chamber. Here, we also verify that the primary atomic beam does not cause a relevant pressure increase in the *Molflow+* simulations, see Fig. 14. Since the rotatable valve is operated by a current source it is possible to keep the channel open only for a couple of seconds for the perticle transfer between the two trap systems, so that the reservoir trap will not experience a significant pressure increase even in the storage time periods of 3 to 6 months.

4 Objectives for the commissioning of the transportable trap

The main objective for BASE-STEP is to develop the transportable trap to a state that it can be used to operate offline experiments with antiprotons latest by the start of LS3. To achieve this, we define the following milestones:

1. **Commissioning of the antiproton injection and accumulation in the former ATRAP I zone.** This concerns the commissioning of a trap system capable of catching and storing antiprotons from the ELENA ejection line. These are established procedures with parameters that have been used

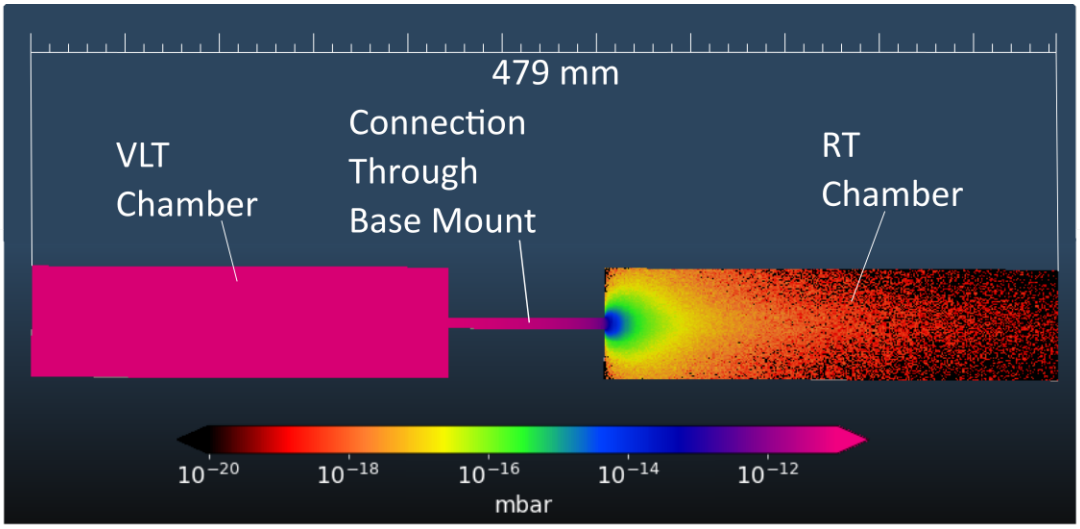

Figure 14: Pressure calculations showing the expansion of the residual gas flow from the VLT chamber at 10^{-11} mbar into the RT chamber. The local pressure of the incoming residual gas at the position of the vacuum lock trap in the center of the VLT chamber is below 10^{-18} mbar.

in the AD [27] except for the degrader system. The progress on the development of the new BASE degrader system has been reported in the BASE annual report 2020. In BASE-STEP, the degrader foil will not be used as a vacuum window and therefore using a commercial 2.0 μm mylar foil will be sufficient to decelerate the antiprotons for catching, and will not require many robustness and permeation tests.
Further, we are interested in quantifying the maximum amount of antiprotons that can be stored during transport, since this will define for which kinds of experiments the transportable trap system could be useful. BASE precision measurements require only a few particles per measurement, however other destructive experiments, such as planned in PUMA [47] or the proposed synthesis of antihydrogen in an rf-trap [18] require to transport larger amounts of antiprotons.

2. **Demonstration of the transportability of the trap system with loaded antiprotons on the CERN Meyrin site.** This will involve training the operation of the system without grid power, and transporting the trap system with antiprotons by crane in the AD hall and on a truck around the Meyrin site of CERN. Here, we will make use of the liquid helium reservoir for the cooling power, while also establishing the operation with a mobile power generator on the truck. An essential part of this study is to investigate the pressure conditions in the trap system as function of time without power and the impact on the stored antiprotons.
3. **Antiproton lifetime studies in the transportable trap system.** This concerns two aspects, the vacuum conditions in the trap system, and the ability to set more stringent limits on antiproton decay channels [24]. To this end, we will store antiprotons and light highly-charged ions, e.g. C^{6+}, in the transportable trap and monitor the number of trapped particles as function of time. This will enable us the make an antiproton-independent vacuum measurement to predict the expected antiproton trap lifetime, and consequently contribute to the exposure time that sets stringent limits on the antiproton decay, as proposed in [24].
4. **Simultaneous cyclotron frequency measurements in BASE-STEP and the BASE apparatus.** Searching for a variation of fundamental constants is an active research area in fundamental physics, since most beyond standard model theories with compactified dimensions induce such time variations. Searches for slow changes in the fine structure constant or in the electron mass have been conducted [3]. Recent interest in these studies is motivated by dark matter models, such as

dilations or relaxions which require searching for fast oscillations [48] or transient variations of fundamental constants due to topological defects in the dark matter structure [25]. Such kind of studies are so far conducted with high precision in the matter sector using atomic clocks or highly-sensitive magnetometers [3]. Searching for transient signals requires in particular a network of clocks (at least two) with uncorrelated noise to search for correlated dark matter signals. So far, spectroscopy on antiprotons and antihydrogen has only been conducted in one experiment. BASE-STEP will enable the first simultaneous antiproton cyclotron frequency measurements, so that the BASE collaboration will be able to demonstrate a transient signal search for dark matter defects by simultaneous frequency measurements in two antiparticle trap systems.

5. **Demonstration of conducting antiproton experiments into a second trap system.** While the first four items will be reached by operating BASE-STEP installed at the ELENA beamport without a second location for a permanent installation, the last item requires a second trap system to which the antiprotons can be transferred and detected. Since the schedule for the BASE experiment is dedicated to antiproton precision measurements until LS3, the BASE apparatus will not necessarily be available for injection of antiprotons from BASE-STEP. To demonstrate the transfer of antiprotons into a second trap system, we are presently preparing a permanent magnet Penning trap in a compact cryostat (70 cm diameter, 1.40 m height) which can be used to receive, store and detect antiprotons from BASE-STEP. The permanent magnet system uses an Aubert magnet configuration [49, 50], which provides more than 200 mT magnetic field in a free space region of 6 cm diameter and 5 cm length [51]. This space is sufficient to install a copy of the vacuum lock trap, so that the feasibility of the transfer can be demonstrated. We will also investigate if this permenent magnet system will be sufficient to work as a second transportable trap.

The SPSC committee has asked whether it is possible to operate BASE-STEP from a shared experiment zone for transportable traps. With the completion of these milestones, the antiproton transportable trap will be prepared to routinely deliver antiprotons to a precision experiment, and will be able to operate with a non-permanent, shared beam port installation in the ELENA facility. As a concept for prioretization and time limitation we propose a shift distribution schedule as earlier used to allocate beamtimes to collaborations in the AD, with equal pro-rata share per user.

5 Technical requirements for the BASE-STEP experimental area

An ECR (EDMS 2464750) has been prepared in coordination with F. Butin about the preparation of the experiment zone [52]. The required modifications to operate BASE-STEP in the former ATRAP I zone is feasible from the infrastructure point of view. The major change requirements to operate BASE-STEP in the experiment area are described below, and further details can be found in the ECR document. The BASE collaboration is able to cover the costs for the required modifications.

Fig. 3 shows the desired layout of the new experiment zone around the former ATRAP I ejection point. The access door and most of the shielding remain in place, however the wall separating the entrance and the ATRAP I magnet area needs to removed, and some shielding elements have to be place between the STEP magnet and the access door since the distance to short without shielding. We propose to place 40 cm thick concrete blocks here leaving 80 cm of space for the zone entrance. The shielding layout was discussed with the RP team (C. Adhiha) and is accepted as solution. BASE-STEP requires power for a cryocooler $8\,\mathrm{kW}$ and a chiller system $< 10\,\mathrm{kW}$, and in addition 4 kW for the operation of vacuum pumps and the trap electronics. The chiller system will cool the compressor of the cryocooler and requires 9 l/min cooling water and deposits $< 10\,\mathrm{kW}$ load into the cooling water system.

6 Project timeline

The superconducting magnet has been ordered and the delivery is foreseen in the time window between October 2021 and April 2022. The offline commissioning of the BASE-STEP trap system will be com-

pleted in 2022. The first online operation in late 2022 and in 2023 would enable to perform the antiproton commissioning and the first transportation tests and to clear the first two objectives. In ELENA it is planned to distribute antiprotons to users on request. Similar to ASACUSA, BASE-STEP and the existing BASE trap system will share the allocated antiproton fraction as one user out of six, together with AEgIS, ALPHA, ASACUSA, GBAR, and PUMA. The remaining objectives (item 3 to 5) are scheduled to be cleared off during the 2024 beamtime.

7 Group structure and funding

At the moment the BASE-STEP team consists of one PI, two PhD students and additional undergraduate students from the University of Mainz. BASE consists of one PI, three post-docs and several PhD students that are permanently stationed at CERN. The equipment for the BASE-STEP trap system is provided by an ERC starting grant (grant no. 852818, 1.8 million EUR, running until 03/2025). Additional funding is available through the BASE collaboration (RIKEN, MPI-K). The transportable trap project is furthermore supported by the Max-Planck, RIKEN, PTB center for time, constants and fundamental symmetries.

Acknowledgements

We are in particluar thankful for the support by F. Butin, M. A. Fraser, Y. Dutheil, W. Bartmann, J. B., C. Carayon, S. Metal, C. Adidha, I. Neuhold, and O. E. Williams, and all other involved persons at CERN for the discussions about the implementation of BASE-STEP. We also acknowledge the support by all CERN teams contributing to antiproton experiments. We acknowledge financial support by the ERC (starting grant no. 852818), RIKEN, the Max-Planck Society, and the QUANTUM group at the Institute of Physics in Mainz.

Bibliography

[1] M. Dine and A, Kusenko. Origin of the matter-antimatter asymmetry. *Rev. Mod. Phys.*, 76:1–30, 2003.

[2] G. Bertone, D. Hooper, and J. Silk. Particle dark matter: evidence, candidates and constraints. *Physics Reports*, 405(5):279–390, 2005.

[3] M. S. Safronova *et al.* Search for new physics with atoms and molecules. *Rev. Mod. Phys.*, 90:025008, 2018.

[4] M. Hori and J. Walz. Physics at cern's antiproton decelerator. *Progress in Particle and Nuclear Physics*, 72:206–253, 2013.

[5] M. Hori *et al.* Buffer-gas cooling of antiprotonic helium to 1.5 to 1.7 K, and antiproton-to–electron mass ratio. *Science*, 354:610–614, 2016.

[6] M. Ahmadi *et al.* Investigation of the fine structure of antihydrogen. *Nature*, 578(7795):375–380, 2020.

[7] M. Ahmadi *et al.* Characterization of the 1s-2s transition in antihydrogen. *Nature*, 557(7703):71–75, 2018.

[8] M. Charlton, S. Eriksson, and G. M. Shore. Testing fundamental physics in antihydrogen experiments. *arXiv*:2002.09348, 2020.

[9] C. Smorra *et al.* A parts-per-billion measurement of the antiproton magnetic moment. *Nature*, 550(7676):371–374, 2017.

[10] S. Ulmer *et al.* High-precision comparison of the antiproton-to-proton charge-to-mass ratio. *Nature*, 524(7564):196–199, 2015.

[11] G. Schneider *et al.* Double-trap measurement of the proton magnetic moment at 0.3 parts per billion precision. *Science*, 358(6366):1081–1084, 2017.

[12] C. Smorra *et al.* Direct limits on the interaction of antiprotons with axion-like dark matter. *Nature*, 575(7782):310–314, 2019.

[13] C. Smorra and A. Mooser. Precision measurements of the fundamental properties of the proton and antiproton. *Journal of Physics: Conference Series*, 1412:032001, 2020.

[14] S. Ulmer *et al.* BASE Annual Report 2019. Technical Report, CERN, Geneva, 2020.

[15] S. Ulmer *et al.* Future Program of the BASE Experiment at the Antiproton Decelerator of CERN. Technical Report CERN-SPSC-2019-047. SPSC-P-363, CERN, Geneva, 2019.

[16] M. Niemann *et al.* Cryogenic ^{9}Be+ Penning trap for precision measurements with (anti-)protons. *Measurement Science and Technology*, 31(3):035003, 2019.

[17] M. Bohman *et al.* Sympathetic cooling of protons and antiprotons with a common endcap penning trap. *Journal of Modern Optics*, 65(5-6):568–576, 2018.

[18] N. Leefer *et al.* Investigation of two-frequency Paul traps for antihydrogen production. *Hyperfine Interactions*, 238(1):12, 2016.

[19] P. Pérez *et al.* The GBAR antimatter gravity experiment. *Hyperfine Interactions*, 233(1):21–27, 2015.

[20] J. Walz and T. W. Hänsch. A proposal to measure antimatter gravity using ultracold antihydrogen atoms. *General Relativity and Gravitation*, 36(3):561–570, 2004.

[21] Hans Dehmelt. Economic synthesis and precision spectroscopy of anti-molecular hydrogen ions in paul trap. *Physica Scripta*, T59:423–423, 1995.

[22] Edmund G. Myers. CPT tests with the antihydrogen molecular ion. *Phys. Rev. A*, 98(1), 2018.

[23] M. J. G. Borge and K. Riisager. HIE-ISOLDE, the project and the physics opportunities. *The European Physical Journal A*, 52(11):334, 2016.

[24] S. Sellner *et al.* Improved limit on the directly measured antiproton lifetime. *New Journal of Physics*, 19(8):083023, 2017.

[25] A. Derevianko and M. Pospelov. Hunting for topological dark matter with atomic clocks. *Nature Physics*, 10(12):933–936, 2014.

[26] M. Takamoto *et al.* Test of general relativity by a pair of transportable optical lattice clocks. *Nature Photonics*, 14(7):411–415, 2020.

[27] C. Smorra *et al.* BASE – The Baryon Antibaryon Symmetry Experiment. *The European Physical Journal Special Topics*, 224(16):3055–3108, 2015.

[28] R. S. Van Dyck *et al.* Ultrastable superconducting magnet system for a penning trap mass spectrometer. *Review of Scientific Instruments*, 70(3):1665–1671, 1999.

[29] J. A. Devlin *et al.* Superconducting solenoid system with adjustable shielding factor for precision measurements of the properties of the antiproton. *Phys. Rev. Applied*, 12:044012, 2019.

[30] G. Gabrielse and J. Tan. Self-shielding superconducting solenoid systems. *Journal of Applied Physics*, 63(10):5143–5148, 1988.

[31] D. J. Fink and E. G. Myers. Deuteron-to-Proton Mass Ratio from the Cyclotron Frequency Ratio of H-2(+) to D+ with H-2(+) in a Resolved Vibrational State. *Phys. Rev. Lett.*, 124(1), 2020.

[32] F. Heisse *et al.* High-Precision Measurement of the Proton's Atomic Mass. *Phys. Rev. Lett.*, 119(3), 2017.

[33] S. Rau *et al.* Penning trap mass measurements of the deuteron and the HD+ molecular ion. *Nature*, 585(7823):43–47, 2020.

[34] R. X. Schüssler *et al.* Detection of metastable electronic states by Penning trap mass spectrometry. *Nature*, 581(7806):42–46, 2020.

[35] R. M. Bass, and M. A. Fraser. Validation of LNE51 AEgIS transfer line optics and electrostatic deflector. CERN Document Server, CERN-ACC-NOTE-2018-0069, 2018.

[36] R. Ostojic, and D. Barna. Electrostatic deflectors (ZDS) forthe elena transfer lines. CERN, EDMS 1410617, LNA-ZQNA-ES-0001, 2017.

[37] R. Ostojic, D. Barna, and W. Bartmann. Electrostatic quadrupole assembly (ZQNA) for elena transfer lines. CERN, EDMS 1410617, LNA-ZDS-ES-0001, 2016.

[38] C. Smorra *et al.* A reservoir trap for antiprotons. *International Journal of Mass Spectrometry*, 389:10–13, October 2015.

[39] M. Block. Direct mass measurements of the heaviest elements with penning traps. *Nuclear Physics A*, 944:471 – 491, 2015. Special Issue on Superheavy Elements.

[40] M. Mukherjee *et al.* ISOLTRAP: An on-line Penning trap for mass spectrometry on short-lived nuclides. *Eur. Phys. J. A*, 35(1):1–29, 2008.

[41] H. Nagahama *et al.* Highly sensitive superconducting circuits at 700 kHz with tunable quality factors for image-current detection of single trapped antiprotons. *Review of Scientific Instruments*, 87(11):113305, 2016.

[42] S. Ulmer *et al.* A cryogenic detection system at 28.9mhz for the non-destructive observation of a single proton at low particle energy. *Nuclear Instruments and Methods in Physics Research Section A*, 705:55–60, 2013.

[43] P. Naik. *Vacuum: Science, Technology & Applications*. Cambridge International S, 2017.

[44] T. Matsuura, A. F. Ismail, and K. C. Khulbe. *Gas Separation Membranes*. Springer International Publishing, 2015.

[45] B. Freeman, Y. Yampolskii, and I. Pinnau. *Materials Science of Membranes for Gas and Vapor Separation*. John Wiley and Sons, Ltd, 2006.

[46] P. S. Yesley. The road to antihydrogen. PhD thesis, Harvard University, 2001.

[47] T. et al. Aumann. Puma: antiprotons and radioactive nuclei. CERN-INTC-2020-003, INTC-I-209, 2020.

[48] D. Antypas *et al.*, Probing fast oscillating scalar dark matter with atoms and molecules, *arXiv*:2012.01519, 2020.

[49] C. Hugon *et al.* Design, fabrication and evaluation of a low-cost homogeneous portable permanent magnet for NMR and MRI. *Comptes Rendus Chimie*, 13(4):388–393, 2010.

[50] D. Sakellariou *et al.* Permanent magnet assembly producing a strong tilted homogeneous magnetic field: towards magic angle field spinning NMR and MRI. *Magnetic Resonance in Chemistry*, 48(12):903–908, 2010.

[51] S. Gavranovic. Design of a vacuum interface and setup of a permanent magnet systemfor the transportable antiproton trap step.

[52] F. Butin, and C. Smorra. ECR: An experimental area at AD for BASE-STEP. CERN, inpreparation.